*Advances in Materials Research, Vol. 1, No. 2 (2012) 115-128*
DOI: http://dx.doi.org/10.12989/amr.2012.1.2.115


# Structural and electrical properties of perovskite $Ba(Sm_{1/2}Nb_{1/2})O_3$–$BaTiO_3$ ceramic

K. Amar Nath[1] and K. Prasad*[2]

[1]*University Department of Physics, T. M. Bhagalpur University, Bhagalpur - 812 007, India*
[2]*Centre for Applied Physics, Central University of Jharkhand, Brambe, Ranchi 835 205, India*

*(Received April 21, 2012, Revised May 17, 2012, Accepted June 3, 2012)*

**Abstract.** The structural and electrical properties of $(1\text{-}x)Ba(Sm_{1/2}Nb_{1/2})O_3$–$xBaTiO_3$; $(0 \le x \le 1)$ ceramics were prepared by conventional ceramic technique at 1375°C/7 h in air atmosphere. The crystal symmetry, space group and unit cell dimensions were derived from the X-ray diffraction (XRD) data using FullProf software whereas crystallite size and lattice strain were estimated from Williamson-Hall approach. XRD analysis of the compound indicated the formation of a single-phase cubic structure with the space group $Pm\bar{3}m$. Dielectric study revealed that the compound $0.75Ba(Sm_{1/2}Nb_{1/2})O_3\text{-}0.25BaTiO_3$ is having low $\varepsilon'$ and $\varepsilon''$ and a low $T_{CC}$ (< 5%) in the working temperature range (up to + 100°C) which makes this composition suitable for capacitor application and may be designated as 'Stable Low-K' Class I material as per the specifications of the Electronic Industries Association. The correlated barrier hopping model was employed to successfully explain the mechanism of charge transport in the system. The *ac* conductivity data were used to evaluate the density of states at Fermi level, minimum hopping length and apparent activation energy of the compounds.

**Keywords:** ceramics; electronic materials; perovskite; lead-free; electrical properties; permittivity; impedance analysis; electrical conductivity

## 1. Introduction

Ceramics with perovskite $ABO_3$ type structures are well known technological materials because of their ability to be employed in a wide variety of applications (Bhalla *et al.* 2000). $BaTiO_3$ is a well-known ferroelectric material with perovskite $ABO_3$-type tetragonal (*p*4 *mm*) structure. It finds widespread applications as a capacitor material because of its high permittivity (~$10^3$). There is an enormous literature on the homovalent, heterovalent ions doped in $BaTiO_3$ either at Ba and/or Ti-site or at both sites, and solid solution of $BaTiO_3$ with other perovskite materials, which showed promising electrical behavior (Li *et al.* 2002, Yuan *et al.* 2004, Hiruma *et al.* 2004, Li *et al.* 2004, Mahboob *et al.* 2006, Umeri *et al.* 2008, Chan *et al.* 2008, Yuan *et al.* 2009). On the other hand, B-site modified $ABO_3$ type materials such as $Ba(Sm_{1/2}Nb_{1/2})O_3$ with cubic ($Pm\bar{3}m$) structure is considered to be a good candidate for microwave applications (Dias *et al.* 2006). Moreover, both the compounds are lead-free and ensure environment-friendly applications. Furthermore, an extensive literature survey suggested that no attempt, to the best of authors' knowledge, has so far

*Corresponding author, Ph. D., E-mail: k.prasad65@gmail.com

been made on the pseudo-binary perovskite type solid-solutions of $Ba(Sm_{1/2}Nb_{1/2})O_3$–$BaTiO_3$ (abbreviated BSN-BT). Both $BaTiO_3$ and $Ba(Sm_{1/2}Nb_{1/2})O_3$ are described as typical perovskite-type compounds and could be expected to form a solid solution. Therefore it is of interest to study the structural and electrical properties of BSN-BT ceramic system. Further, complex impedance analysis has proved to be a powerful technique to estimate the influence of grain, grain boundary and electrode effects on the charge transport phenomenon in perovskite materials. Accordingly, the present work aim to study the structural (X-ray and their Rietveld analyses), microstructural, electrical (dielectric, impedance, *ac* conductivity) properties of $(1\text{-}x)Ba(Sm_{1/2}Nb_{1/2})O_3$–$xBaTiO_3$ ceramics with different composition ($x$ = 0, 0.25, 0.50, 0.75 and 1.0). Also, an attempt has been made to understand the conductions mechanism in the system using correlated barrier hopping model. The *ac* conductivity data have been used to estimate the apparent activation energy, density of states at Fermi level and minimum hopping length. The results on dielectric properties indicated that the compound $Ba(Sm_{1/2}Nb_{1/2})_{0.75}Ti_{0.25}O_3$ meets the specifications for 'Stable Low-K' Class I dielectrics of Electronic Industries Association, USA.

## 2. Experimental details

Polycrystalline samples of $(1\text{-}x)Ba(Sm_{1/2}Nb_{1/2})O_3$–$xBaTiO_3$; $x$ = 0, 0.25, 0.50, 0.75 and 1.0 were prepared from AR grade (99.9%+ pure, Merck) chemicals ($BaCO_3$, $Sm_2O_3$, $Nb_2O_5$ and $TiO_2$) using solid-state synthesis at 1375°C for 7 h under a controlled heating and cooling cycles. Circular disc shaped pellets having geometrical dimensions: thickness ≈ 1.4 mm and diameter ≈ 10 mm were made by applying uniaxial stress of 650 MPa. The pellets were subsequently heated up to 1400°C under air atmosphere for 5 h. The completion of reactions and the formation of desired compounds were checked by X-ray diffraction.

The X-ray diffraction (XRD) spectra were taken on sintered pellets of BSN-BT with a X-ray diffractometer (XPERT-PRO, Pan Analytical) at room temperature, using $CuK_a$ radiation ($\lambda$ = 1.5406 Å), over a wide range of Bragg angles ($20^o \leq 2\theta \leq 90^o$) with a scanning speed of $5.08^o$ $min^{-1}$. The *XY* ($2\theta$ vs. intensity) data were plotted with the WinPLOTR program and the angular positions of the peaks were obtained with the same program. The dimensions of the unit cell, *hkl* values and space group of BSN-BT were obtained using the TREOR program in the FullProf 2000 software. The refinements were carried out through the profile matching routine of FullProf. The Bragg peaks were modeled with pseudo-Voigt function and the backgrounds were estimated by linear interpolation between selected background points.

The real ($Z'$) and imaginary ($Z''$) parts of the electrical impedance of all the compounds were measured as functions of frequency (1 Hz - 1 MHz) and temperature (50°C - 450°C) using a computer-controlled impedance/gain-phase analyzer (Solartron SI 1260) in a cooling mode on a symmetrical cell of type Ag|*Ceramic*|Ag, where Ag is a conductive paint coated on either side of the pellets. The temperature was varied at a rate of 1°C/min.

## 3. Theoretical background

The crystallite size ($D$) and the lattice strain ($\Delta\xi/\xi$) of BSN-BT ceramics were estimated by analyzing the broadening of X-ray diffraction peaks, using Williamson-Hall approach.

$$B\cos\theta = (K\lambda/D) + 2(\Delta\xi/\xi)\sin\theta \tag{1}$$

where $B$ is diffraction peak width at half intensity and $K$ is the Scherrer constant (0.89). The term $K\lambda/D$ represents the Scherrer particle size distribution. The real ($\varepsilon'$) and imaginary ($\varepsilon''$) parts of permittivity were obtained from the impedance data using the following relations

$$\varepsilon'(\omega) = Z''/\omega C_o|Z^*|^2 \tag{2}$$

$$\varepsilon''(\omega) = Z'/\omega C_o|Z^*|^2 \tag{3}$$

where $|Z| = [(Z')^2 + (Z'')^2]^{1/2}$. Further, the temperature coefficient of capacitance ($T_{CC}$) which is an important parameter for the low-temperature dependence of capacitance is defined as

$$T_{CC}(\%) = \frac{C_T - C_{RT}}{C_{RT}} \times 100 \tag{4}$$

The *ac* conductivity data was obtained using the relation $\sigma^*(\omega) = \sigma'(\omega) + i\sigma''(\omega) = i\omega\varepsilon_o\varepsilon^*(\omega)$ and the real ($\sigma'$) and imaginary ($\sigma''$) parts of $\sigma^*(\omega)$ were obtained as

$$\sigma'(\omega) = \omega\varepsilon_o\varepsilon''(\omega) \tag{5}$$

$$\sigma''(\omega) = \omega\varepsilon_o\varepsilon'(\omega) \tag{6}$$

The *ac* electrical conductivity, in most of the materials due to localized states is given by

$$\sigma'(\omega) = \sigma_o + A\omega^s \tag{7}$$

where $\sigma_o$ is the frequency-independent (electronic or *dc*) part of *ac* conductivity, $s$ ($0 \le s \le 1$) is the index, $\omega$ is angular frequency of applied *ac* field and $A$ [$= \pi N^2 e^2/6k_BT\ (2\alpha)$] is a constant, $e$ is the electronic charge, $T$ is the temperature, $\alpha$ is the polarizability of a pair of sites and $N$ is the number of sites per unit volume among which hopping takes place. Such variation is associated with displacement of carriers which move within the sample by discrete hops of length $R$ between randomly distributed localized sites. The term $A\omega^s$ can often be explained on the basis of two distinct mechanisms for carrier conduction: (a) quantum mechanical tunnelling (QMT) through the barrier separating the localized sites and (b) correlated barrier hopping (CBH) over the same barrier. In these models, the exponent $s$ is found to have two different trends of variation with temperature and frequency. In QMT, $s$ is predicted to be temperature independent and is expected to show a decreasing trend with $\omega$

$$s = 1 + 4/\log(\omega\tau_o) \tag{8}$$

where $\tau_o$ is the characteristic relaxation time. The *ac* conductivity is expected to follow the relationship (Elliott 1987)

$$\sigma' = \frac{\pi^4}{24} e^2 \omega k_B T[N(E_f)]^2 \alpha^{-1} R_\omega^4 \tag{9}$$

where $\alpha^{-1}$ is the spatial decay parameter for the localized wave function and $R_\omega$ is the tunnelling length at frequency $\omega$

$$R_\omega = \frac{1}{2\alpha}\ln(1/\omega\tau_o) \tag{10}$$

Further, if *ac* conductivity occurs from CBH, the *ac* conductivity data should follow the relationship (Sharma *et al.* 2003)

$$\sigma' = \frac{\pi}{3} e^2 \omega k_B T [N(E_f)]^2 \alpha^{-5} [\ln(f_o/\omega)]^4 \tag{11}$$

where $N(E_f)$ is the density of states at Fermi level, $f_o$ the photon frequency and $\alpha$ is the localized wave function. The exponent $s$ and minimum hopping length, $R_{\min}$ can be expressed as (Mollah *et al.* 1993, Salam 1990)

$$s = 1 - (6k_B T/W_m) \tag{12}$$

$$R_{\min} = 2e^2/\pi\varepsilon\varepsilon_o W_m \tag{13}$$

where $W_m$ is the binding energy, which is defined as the energy required to remove an electron from one site to the another site.

## 4. Results and discussion

### 4.1 Structural and microstructural studies

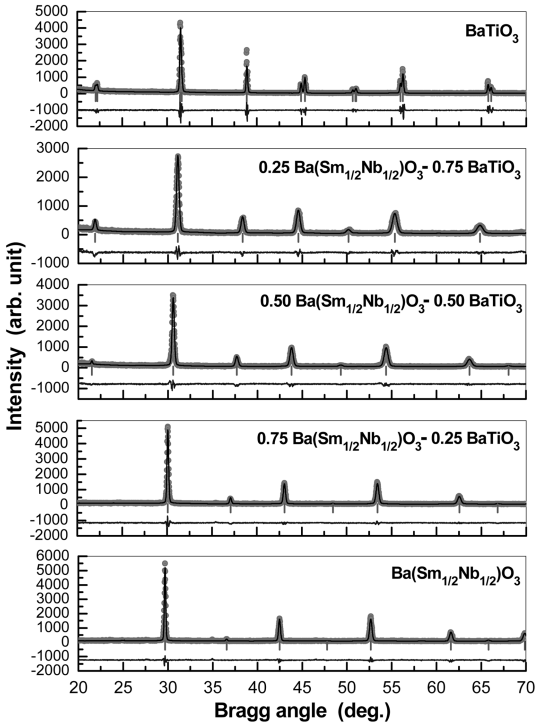


Fig. 1 Rietveld refined patterns of (1-$x$)Ba($Sm_{1/2}Nb_{1/2}$)$O_3$–$x$$BaTiO_3$; $x$ = 0, 0.25, 0.50, 0.75 and 1.0 ceramics. Symbols represent the observed data points, the solid lines their Rietveld fit, vertical lines their Bragg positions and lower solid lines their difference (observed-calculated data) profile

Table 1 The crystal data and refinement factors obtained from X-ray powder diffraction data of (1-$x$)Ba($Sm_{1/2}Nb_{1/2}$)$O_3$–$x$$BaTiO_3$; $x$ = 0, 0.25, 0.50, 0.75 and 1.0 ceramics

| Parameters | $x$ = 0 | $x$ = 0.25 | $x$ = 0.50 | $x$ = 0.75 | $x$ = 1.0 |
|---|---|---|---|---|---|
| Crystal system | Cubic | Cubic | Cubic | Cubic | Tetragonal |
| Space group | $Pm\bar{3}m$ (221) | $Pm\bar{3}m$ (221) | $Pm\bar{3}m$ (221) | $Pm\bar{3}m$ (221) | $P/4mm$ (99) |
| $a$ (Å) | 4.2540 | 4.1968 | 4.1297 | 4.0628 | 3.9956 |
| $b$ (Å) | --- | --- | --- | --- | 3.9956 |
| $c$ (Å) | --- | --- | --- | --- | 4.0310 |
| $V$ (Å$^3$) | 76.9822 | 73.9187 | 70.4310 | 67.0633 | 64.3535 |
| $R_p$ | 29.8 | 26.0 | 26.0 | 23.2 | 40.7 |
| $R_{wp}$ | 26.7 | 23.4 | 24.0 | 22.5 | 41.1 |
| $R_{exp}$ | 16.3 | 16.1 | 16.1 | 15.1 | 16.6 |
| $R_B$ | 0.177$E$-3 | 0.192$E$-3 | 0.444$E$-3 | 0.133$E$-3 | 5.59 |
| $R_F$ | 0.194$E$-3 | 0.168$E$-3 | 0.434$E$-3 | 0.740$E$-3 | 4.08 |
| $\chi 2$ | 2.698 | 2.107 | 2.228 | 2.232 | 6.113 |
| $d$ | 1.1568 | 1.2784 | 1.1314 | 1.1823 | 0.657 |
| $Q_D$ | 1.8859 | 1.8889 | 1.8846 | 1.8784 | 1.8716 |
| $S$ | 1.638 | 1.4534 | 1.4907 | 1.4901 | 2.48 |

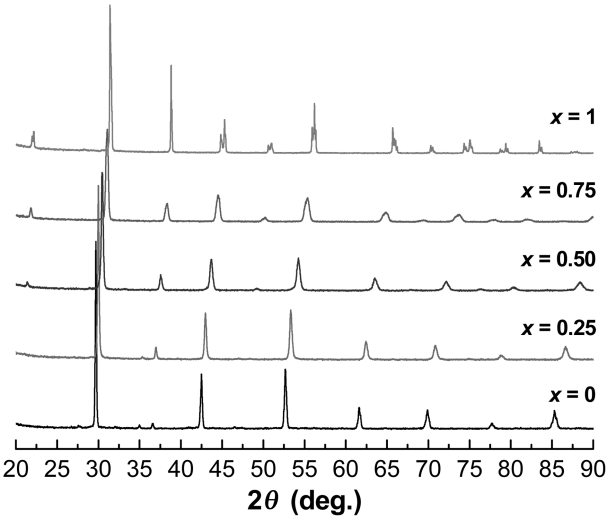


Fig. 2 X-ray diffraction patterns of (1-$x$)Ba($Sm_{1/2}Nb_{1/2}$)$O_3$–$x$$BaTiO_3$; $x$ = 0, 0.25, 0.50, 0.75 and 1.0 ceramics showing the shifting of different peaks

With an aim to see the effect of $BaTiO_3$ addition to Ba($Sm_{1/2}Nb_{1/2}$)$O_3$ on the unit cell structure, Rietveld analyses of (1-$x$)Ba($Sm_{1/2}Nb_{1/2}$)$O_3$–$x$$BaTiO_3$; $x$ = 0, 0.25, 0.50, 0.75 and 1.0 have been carried out. Fig. 1 illustrates the observed, calculated and difference profiles for BFN-BT after final cycles of refinements. Appearance of single and sharp peaks of all the compounds and no other peaks due to any component oxides/carbonates indicated the formation of single phase compounds. It can be seen that the profiles for observed and calculated one are perfectly matching. The profile fitting procedure adopted was minimizing the $\chi^2$ function. The crystal data and refinement factors of BSN-BT obtained from XRD data are depicted in Table 1. The compounds show a single cubic

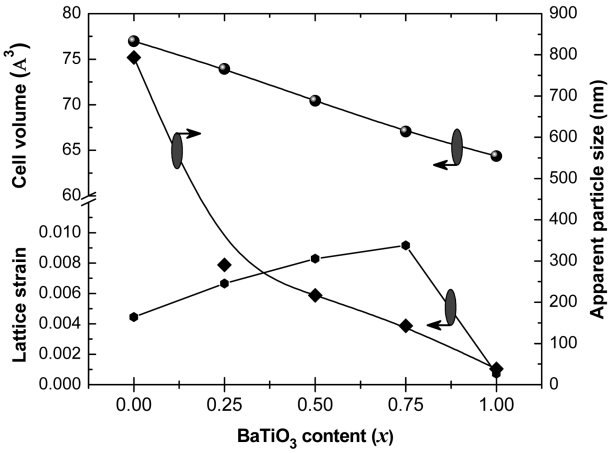


Fig. 3 Compositional dependence of unit cell volume, lattice strain and apparent particle size of (1-$x$)Ba($Sm_{1/2}Nb_{1/2}$)$O_3$–$x$$BaTiO_3$; $x$ = 0, 0.25, 0.50, 0.75 and 1.0 ceramics

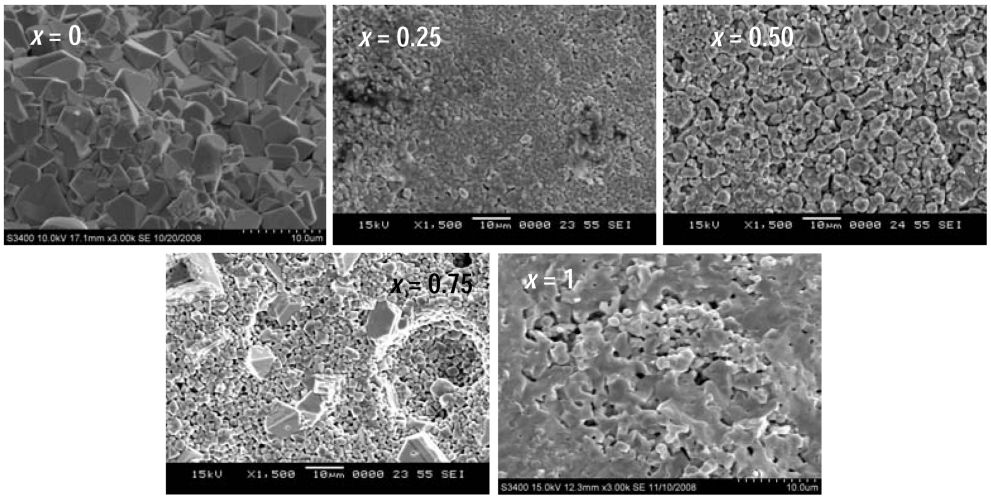


Fig. 4 SEM micrographs of fractured surface of (1-$x$)Ba($Sm_{1/2}Nb_{1/2}$)$O_3$–$x$$BaTiO_3$; $x$ = 0, 0.25, 0.50, 0.75 and 1.0 ceramics

phase formation with space group $Pm\bar{3}m$ (221) except $BaTiO_3$ for which the unit cell structure comes out to be tetragonal. Therefore, addition of $BaTiO_3$ could not change the basics unit cell structure of the solid-solutions. This could be due to the highly tolerant structure (tolerance factor = 0.97272) of Ba($Sm_{1/2}Nb_{1/2}$)$O_3$. However, some shifting in the peak positions and changes in the intensities of peaks could be observed (Fig. 2). Further, a linear least square fitting to $B\cos\theta$–$\sin\theta$ data yielded the values of average crystallite size and lattice strain in the compounds. Fig. 3 shows the compositional variation of unit cell volume, lattice strain and apparent particle size of BSN-BT ceramics. A decrease in the unit cell volume and apparent particle size is observed with the increasing $BaTiO_3$ content ($x$). A linear least square fitting to concentration dependence unit cell volume data yielded the relation: $V = 76.9723 - 18.84512x$ with $r^2 = 0.99786$. Also an increase in

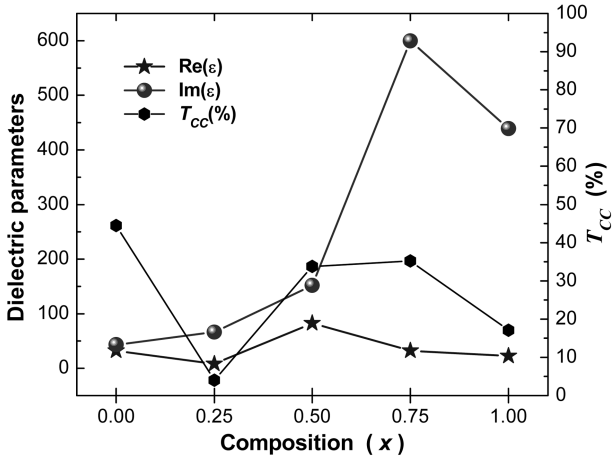


Fig. 5 Compositional variation of dielectric parameters of (1-$x$)$Ba(Sm_{1/2}Nb_{1/2})O_3$–$xBaTiO_3$; $x$ = 0, 0.25, 0.50, 0.75 and 1.0 ceramics

lattice strain with the increment in $x$ is observed (Fig. 3), which could be due to the partial replacement of pseudo-cation $(Sm^{3+}_{1/2}Nb^{5+}_{1/2})^{4+}$ with $Ti^{4+}$ which produces some kind of disorder in the system and/or due to the difference in unit cell structure of $Ba(Sm_{1/2}Nb_{1/2})O_3$ (cubic) and $BaTiO_3$ (tetragonal). Besides, the difference in the ionic radii of pseudo-cation $(Sm^{3+}_{1/2}Nb^{5+}_{1/2})^{4+}$ and $Ti^{4+}$ might have played an important role.

Fig. 4 shows the scanning electron micrographs of the fractured surface of BSN-BT ceramics. The photographs contain a very few voids suggesting the high density of the materials. The grains of unequal sizes (1-5 $\mu$m) appear to be distributed throughout the samples. It is also observed that a few number of grains are agglomerated, grow rapidly to a larger size relative to the average size which is termed as an abnormal grain growth or secondary crystallization. The ratio of the average particle size to the grain size for all the compositions is found to be of the order of $10^{-3}$.

### *4.2 Dielectric study*

Fig. 5 shows the compositional dependence of $\varepsilon'$, $\varepsilon''$ and $T_{CC}$(%) for BSN-BT ceramics at room temperature. It can be seen that the value of $\varepsilon''$ increases with the increment in BT content ($x$) and is maximum for $x$ = 0.75. It is well known that $BaTiO_3$ is an established material for capacitor applications. Also, it is observed that the addition of BT to BSN, in general, lowers the value of $T_{CC}$. The low values of $\varepsilon'$ (= 66.26), $\tan\delta$ (= $\varepsilon''/\varepsilon'$ = 0.12) as well as $T_{CC}$ (< ±5%) in the working temperature range (up to +100°C) for $Ba(Sm_{1/2}Nb_{1/2})_{0.75}Ti_{0.25}O_3$ are found, which meets the specifications for "Stable Low-K" Class I dielectrics of Electronic Industries Association, USA (Moulson and Herbert 2003). Therefore, adding 25% $BaTiO_3$ to $Ba(Sm_{1/2}Nb_{1/2})O_3$ led to the mark improvement in $T_{CC}$. Hence, this compound may consider being a potential candidate for capacitor applications.

### *4.3 Complex impedance study*

Fig. 6 shows the variation of room temperature values of $Z'$ and $Z''$ and the activation energy

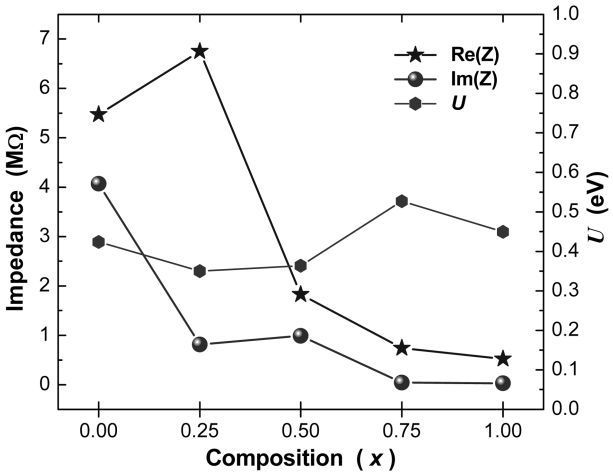


Fig. 6 Compositional variation of real and imaginary parts of impedance and activation energy of (1-$x$)Ba($Sm_{1/2}Nb_{1/2}$)$O_3$–$x$$BaTiO_3$; $x$ = 0, 0.25, 0.50, 0.75 and 1.0 ceramics

($U$) with concentration ($x$) for BSN–BT. It is observed that addition of $BaTiO_3$ to Ba($Sm_{1/2}Nb_{1/2}$)$O_3$ ceramic, in general, led to the decrease in real and imaginary parts of impedance. Also it is noted that the value of $Z'$ (= 8.16 MΩ) is found highest for Ba($Sm_{1/2}Nb_{1/2}$)$_{0.75}Ti_{0.25}O_3$, which is considered to be advantageous for capacitor applications. Also, the relaxation time was estimated from $Z''$ vs. frequency plots at which $Z''_{max}$ is observed. At the peak ($\omega = \omega_o$), the most probable relaxation is defined by the condition

$$\omega \tau = 1 \tag{14}$$

where $\tau$ is the relaxation time and obey the Arrhenius relationship

$$\tau = \tau_o \exp(-U / k_B T) \tag{15}$$

where $\tau_o$, $U$, $k_B$ and $T$ are the pre-exponential factor, activation energy, Boltzmann constant and absolute temperature, respectively. The values of $U$ were estimated using linear least square fit to the $\log\tau$ vs. $1/T$ data. The highest value of activation energy is found for $x$ = 0.75.

### 4.4 AC conductivity studies

Fig. 7 illustrates the variation of σ′ and σ″ as a function of frequency at different temperatures for BSN-BT ceramics. It is observed that the patterns of the *ac* conductivity spectrum show dispersion throughout the chosen frequency range and with the rise in temperature, the nature of conductivity spectrum appears to be changed. The low frequency plateau becomes almost frequency independent at higher temperatures and the frequency dependence of real part of *ac* conductivity obeys Eq. 7, the Jonscher's power law (Jonscher 1983). The values of the index $s$ can be obtained from the slopes of the plots ($\log\sigma'$ vs. $\log f$). Insets of Fig. 7 show the variation of $s$ with temperature. It can be seen that the values of $s$ are always less than 1 and it decreases with the rise of temperature for all the compounds. Besides, the value of $s \rightarrow 0$ at higher temperatures, indicates that the *dc* conductivity dominates at higher temperatures in the low frequency region and following

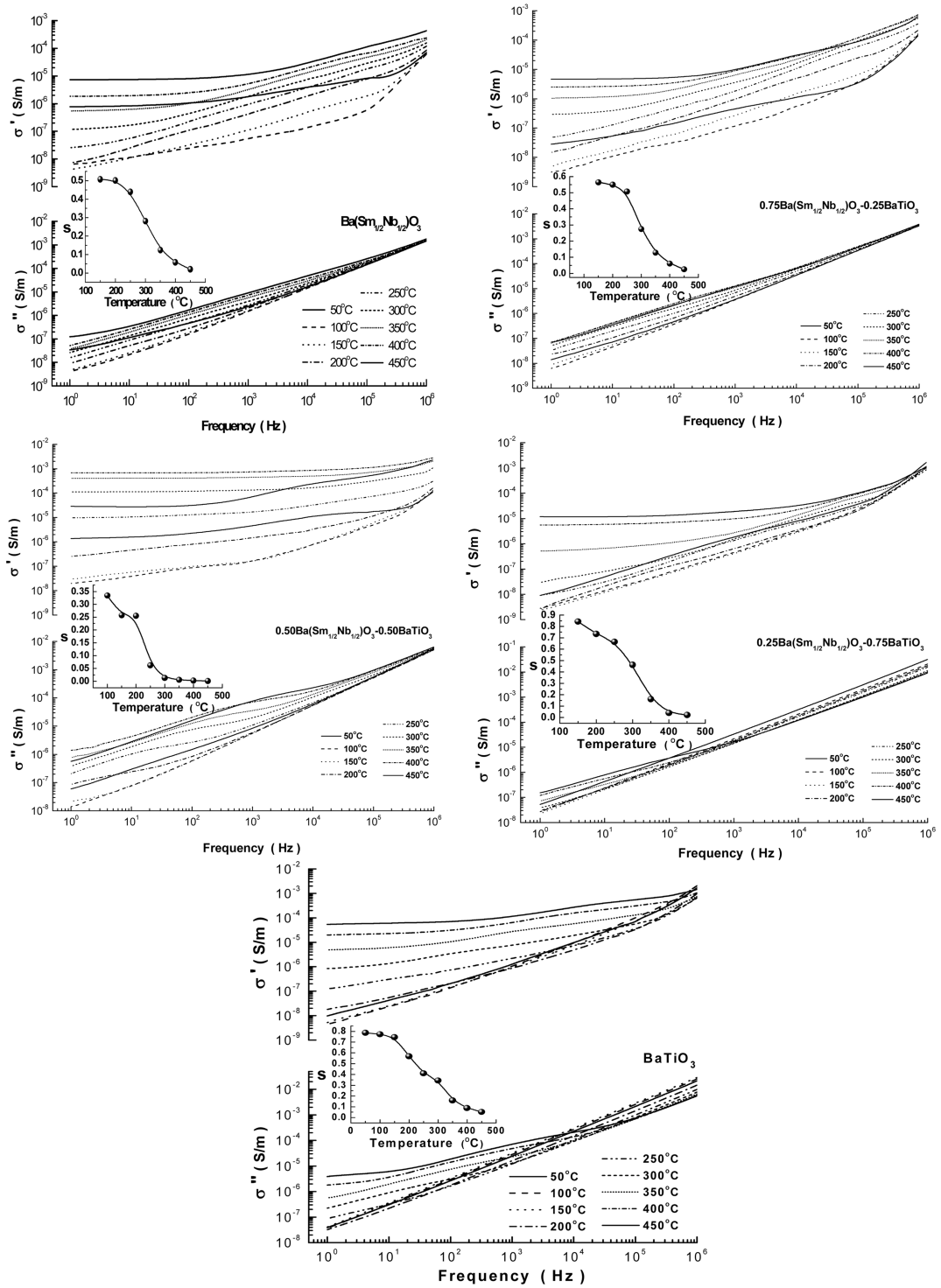


Fig. 7 Variation of real and imaginary parts of *ac* conductivity of (1-*x*)$Ba(Sm_{1/2}Nb_{1/2})O_3$–*x*$BaTiO_3$; *x* = 0, 0.25, 0.50, 0.75 and 1.0 with frequency at different temperatures. Inset: Temperature variation of index *s*

Eq. (8). The model based on correlated barrier hopping of electrons predicts a decrease in the value of the index with the increase in temperature (Elliott 1978). The experimental results follow the same trend. Therefore, the conduction in the system could be considered due to the short-range translational type hopping of charge carriers (Elliott 1978, Funke 1993). Also, it is observed that the slope of the curves change with the temperature, which clearly indicates that the conduction process is dependent on both temperature and frequency. The frequency, at which there is a slope change, shifts to higher frequency side upon increasing temperature. The switch from the frequency-independent to the dependent regions show the onset of the conductivity relaxation phenomenon and the translation from long range hopping to the short range ion motion (Mizaras *et al.* 1997). Such dependence is associated with displacement of carriers which move within the sample by discrete hops of length $R$ between randomly distributed localized sites.

Furthermore, a decrease in the values of $\sigma'$ is observed with the rise in temperature for all the compounds, thereby indicating the negative temperature coefficient of resistance (NTCR) character of the samples like that of semiconductors. This may happen due to the accumulation of charge species at the barriers (grain boundaries) which get thermally activated, that plays a dominant role at elevated temperature showing NTCR characteristics. With the rise in temperature, these charge species have sufficient energy to jump over the barrier, thereby increasing the conductivity and hence the grain boundary resistance decreases beyond these temperatures. The increase in conductivity with temperature may be considered on the basis that within the bulk, the oxygen vacancies due to the loss of oxygen are usually created during sintering. It is known that in perovskite titanates, ionization of oxygen vacancy creates conducting electrons, a process which can be described using the Kröger and Vink notation (Kröger and Vink 1956). These excess electrons and oxygen vacancies are formed in the reduction reaction during sintering that enhances the electrical conductivity, dielectric loss and space charge accumulation at the grain boundaries which are detrimental to the material's performance (Maier *et al.* 2001, Bhagat and Prasad 2010). It is reported that titanate based perovskite oxide materials contain $Ti^{3+}$ that are formed because of capture of electron released during the process of formation of oxygen vacancies by $Ti^{4+}$. The polaronic conduction of 3*d* electrons on $Ti^{3+}$ with low mobility must be predominant at low temperature and these polaronic states are thermally dissociated and the residual carriers, 3*d* electrons, are strongly scattered by thermal phonons at high temperature, resulting in high electronic conductivity (Iguchia and Mochizuki 2004). In BSN-BT system, partial replacement of $Ti^{4+}$ ions with $Sm^{3+}$ and $Nb^{5+}$ ions may result in localized oxygen vacancies and titanium vacancies given as: $12BaO + 3Sm_2O_3 + 2Nb_2O_5 + TiO_2 \rightarrow 12Ba + Ti + 6Sm_{Ti} + 4Nb_{Ti} + 33O + 3V_o + V_{Ti}$, where $V_O$ and $V_{Ti}$ are, respectively, the oxygen and titanium vacancies. $Sm_{Ti}$ and $Nb_{Ti}$ respectively, represent the incorporation of Sm and Nb at Ti position. Since Ti can exist in +3 and +4 state, whereas Nb can exist in +4 and +5 states, $Ti^{4+}$ and $Nb^{5+}$ ions may capture the electrons to form $Ti^{3+}$ and $Nb^{5+}$ ions, respectively. The polaronic conduction of 3*d* electrons on $Ti^{3+}$ and 4*d* electrons on $Nb^{5+}$ with low mobility may be predominant at intermediate temperature. These polaronic states may be thermally dissociated and the residual carriers, 3*d* and 4*d* electrons are strongly scattered by thermal phonons at high temperature, resulting in high electronic conductivity. High electronic conductivity at elevated temperatures may also be attributed to the increase in polaronic conduction. This increase in polaronic conduction may be linked to the formation of more oxygen vacancies due to oxygen loss at very high temperatures. Such type of hopping polaronic conduction has been reported in disordered perovskite, $Sr_{0.97}(Ti_{1-x}Fe_x)O_{3-d}$ (Ang *et al.* 1998). Contribution to the polaronic conduction from Sm-ion can be ruled out, as it has stable valence state, +3. In the present

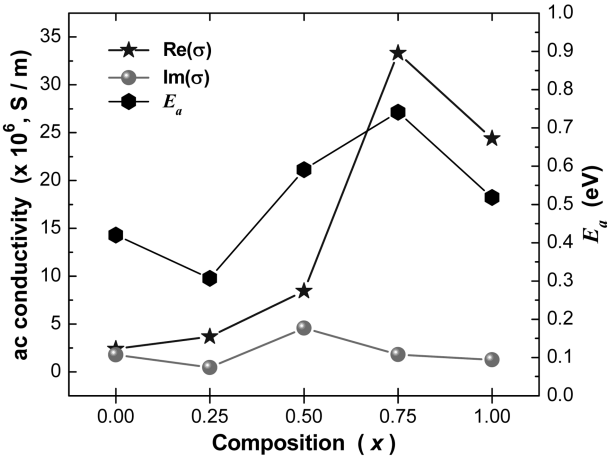


Fig. 8 Compositional ($x$) variation of real and imaginary parts of *ac* conductivity at room temperature and activation energy of (1-$x$)$Ba(Sm_{1/2}Nb_{1/2})O_3$–$xBaTiO_3$; $x$ = 0, 0.25, 0.50, 0.75 and 1.0

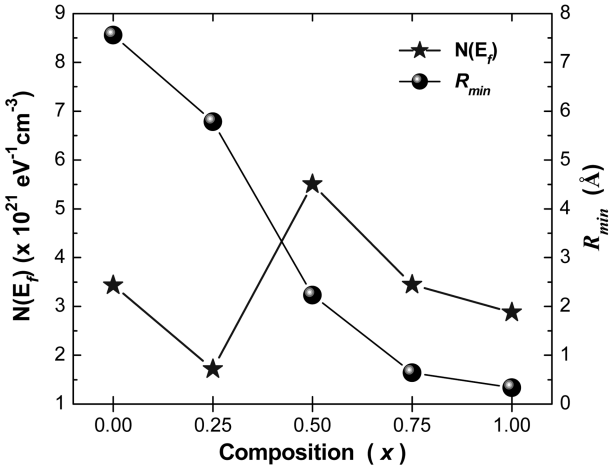


Fig. 9 Compositional ($x$) variation of $N(E_f)$ and $R_{min}$ at room temperature of (1-$x$)$Ba(Sm_{1/2}Nb_{1/2})O_3$–$xBaTiO_3$; $x$ = 0, 0.25, 0.50, 0.75 and 1.0

perovskite oxide materials the high frequency localized orientation hopping may be attributed to the formation of dipoles, $Nb^{5+}-V_O$ and $Ti^{3+}-V_O'$. These dipoles can change their orientations by electron hopping. The hopping of 4*d* electrons, $Nb^{5+}-V_O$ and $Ti^{3+}-V_O'$, gives rise to localized energy levels in the energy gap of $Ba[(Sm_{1/2}Nb_{1/2})_{1-x}Ti_x]O_3$. The charge carriers trapped at these localized sites may form large polarons and conduction occurs as a result of thermally activated large polarons. This is also clear from the temperature dependence of $s$, which decreases with increasing temperature for hopping mechanism of large polarons (Elliott 1987, Upadhyay *et al.* 1998).

Fig. 8 shows the compositional ($x$) variation of room temperature values of $\sigma'$ and $\sigma''$ and the apparent activation energy ($E_a$). It can be seen that the value of $\sigma'$ increases with the increment in $x$ and is maximum for $x$ = 0.75. The values of $E_a$ were estimated using the linear fitting of $\log\sigma'$ vs.

$1/T$ data. The minimum and maximum values of $E_a$ are observed in case of $x$ = 0.25 and 0.75, respectively. The low values of $E_a$ might be due to the transport of charge carriers through hopping between localized states in a disordered manner (Prasad *et al.* 2006).

Hopping conduction mechanism is generally consistent with the existence of a high density of states in the materials having band gap like that of semiconductor. Due to localization of charge carriers, formation of polarons takes place and the hopping conduction may occur between the nearest neighboring sites. Based on CBH model, the *ac* conductivity data have been used to evaluate the density of states at Fermi level $N(E_f)$ using the relation Eq. (11) assuming $f_o = 10^{13}$ Hz and $\alpha = 10^{10}\,m^{-1}$ and $R_{min}$ (minimum hopping length) at various operating frequencies and temperatures. Fig. 9 depicts compositional ($x$) variation of $N(E_f)$ and $R_{min}$ of BSN-BT ceramics at room temperature. It is observed that the value of $N(E_f)$ found minimum for $Ba(Sm_{1/2}Nb_{1/2})_{0.75}Ti_{0.25}O_3$., which is consistent with the results of dielectric and impedance data. The reasonably high values of $N(E_f)$ suggest that the hopping between the pairs of sites dominate the mechanism of charge transport in these compounds. It is observed that the value of $R_{min}$ decreases upon increasing $BaTiO_3$ content ($x$). Also, it is characterized by a very low value ~$10^{-10}$ m and is found to be ~$10^{-4}$ times smaller in comparison to the grain size of all the compounds.

## 5. Conclusions

Polycrystalline $(1\text{-}x)Ba(Sm_{1/2}Nb_{1/2})O_3$–$xBaTiO_3$; $(0 \le x \le 1)$ prepared using a high-temperature solid-state reaction technique, were found to have a perovskite-type cubic structure with the space group $Pm\bar{3}m$ except $BaTiO_3$ (tetragonal, $P4\,mm$). Dielectric study revealed that the compound $0.75Ba(Sm_{1/2}Nb_{1/2})O_3$-$0.25BaTiO_3$ is having low $\varepsilon'$ and $\varepsilon''$ and a low $T_{CC}$ (< 5%) in the working temperature range (up to +100°C) which makes this composition suitable for capacitor application and may be designated as 'Stable Low-K' Class I material as per the specifications of the Electronic Industries Association. The *ac* conductivity study showed the NTCR character of the compounds. The *ac* conductivity is found to obey the universal power law and the correlated barrier hopping model is found to successfully explain the mechanism of charge transport in the system. These results are well supported by density of states at Fermi level and minimum hopping length data. The value of minimum hopping length was found to be ~$10^{-4}$ times smaller in comparison to the grain size.

## Acknowledgements

The present work was supported by ER & IPR Division of Defense Research and Development Organization, New Delhi. Authors acknowledge Prof. A.R. Kulkarni, Indian Institute of Technology, Mumbai, India for providing generous experimental support and Dr. K.P. Chandra, S.M. College, Bhagalpur, India for help in experimentation and fruitful discussion.

## References

Ang, C., Jurado, J.R., Yu, Z., Colomer, M.T., Frade, J.R. and Baptista, J.L. (1998), "Variable-range-hopping

conduction and dielectric relaxation in disordered $Sr_{0.97}(Ti_{1-x}Fe_x)O_{3-\delta}$", *Phys. Rev.* B, **57**(19), 11858-11861.
Bhagat, S. and Prasad, K. (2010), "Structural and impedance spectroscopy analysis of $Ba(Fe_{1/2}Nb_{1/2})O_3$ ceramic", *Phys. Status Solidi A*, **207**(5), 1232-1239.
Bhalla, A.S., Guo, R. and Roy, R. (2000), "The perovskite structure – a review of its role in ceramic science and technology", *Mater. Res. Innov.*, **4**(1), 3-26.
Chan, H.L.W., Choy, S.H., Chong, C.P., Li, H.L. and Liu, P.C.K. (2008), "Bismuth sodium titanate based lead-free ultrasonic transducer for microelectronics wirebonding applications", *Ceram. Int*., **34**(4), 773-777.
Dias, A., Abdul Khalam, L., Sebastian, M.T., Paschoal, C.W.A. and Moreira, R.L. (2006), "Chemical substitution in $Ba(RE_{1/2}Nb_{1/2})O_3$ (RE = La, Nd, Sm, Gd, Tb, and Y) microwave ceramics and its influence on the crystal structure and phonon modes", *Chem. Mater.*, **18**(1), 214-220.
Elliott, S.R. (1978), "Temperature-dependence of ac conductivity of chalcogenide glasses", *Philos. Mag. B*, **37**(5), 553-560.
Elliott, S.R. (1987), "A.c. conduction in amorphous chalcogenide and pnictide semiconductors", *Adv. Phys*., **36**(2), 135-217.
Funke, K. (1993), "Jump relaxation in solid electrolytes", *Prog. Solid State Ch*., **22**, 111-195.
Hiruma, Y., Aoyaqi, R., Nagata, H. and Takenaka, T. (2004), "Piezoelectric properties of $BaTiO_3$–$(Bi_{1/2}K_{1/2})TiO_3$ ferroelectric ceramics", *Jpn. J. Appl. Phys*., **43**(11), 7556-7559.
Iguchia, E. and Mochizuki, S. (2004), "Electric conduction and dielectric relaxation processes in solid oxide fuel cell electrolyte $La_{0.5}Sr_{0.5}Ga_{0.6}Ti_{0.4}O_{3\delta}$", *J. Appl. Phys*., **96**(7), 3889-3896.
Jonscher, A.K. (1983), *Dielectric relaxation in solids*, Chelsea, New York.
Kröger, F.A. and Vink, H.J. (1956), "Relations between the concentrations of imperfections in crystalline solids", *Solid State Phys*., **3**(3), 307-435.
Li, G., Liu, S., Liao, F., Tian, S., Jing, X., Lin, J., Uesu, Y., Kohn, K., Saitoh, K., Terauchi, M., Di, N. and Cheng, Z. (2004), "The structural and electric properties of the perovskite system $BaTiO_3$-$Ba(Fe_{1/2}Ta_{1/2})O_3$", *J. Solid State Chem*., **177**(4-5), 1695-1703.
Li, W., Qi, J., Wang, Y., Li, L. and Gui, Z. (2002), "Doping behaviors of $Nb_2O_5$ and $Co_2O_3$ in temperature stable $BaTiO_3$-based ceramics", *Mater. Lett*., **57**(1), 1-5.
Mahboob, S., Dutta, A.B., Prakash, C., Swaminathan, G., Suryanarayana, S.V., Prasad, G. and Kumar, G.S. (2006), "Dielectric behaviour of microwave sintered rare-earth doped $BaTiO_3$ ceramics", *Mater. Sci. Eng. B*, **134**(1), 36-40.
Maier, R., Chon, J.L., Neumeier, J.J. and Bendersky, L.A. (2001), "Ferroelectricity and ferrimagnetism in iron-doped $BaTiO_3$", *Appl. Phys. Lett*., **78**(17), 2536-2539.
Mizaras, R., Takashige, M., Banys, J., Kojima, S., Grigas, J., Hamazaki S.I. and Brilingas, A. (1997), "Dielectric relaxation in $Ba_2NaNb_{5(1-x)}Ta_{5x}O_{15}$ single crystals", *J. Phys. Soc. Jpn.*, **66**(9), 2881-2885.
Mollah, S., Som, K.K., Bose, K. and Chaudri, B.K. (1993), "ac conductivity in $Bi_4Sr_3Ca_3Cu_yO_x$ ($y$ = 0–5) and $Bi_4Sr_3Ca_{3z}Li_zCu_4O_x$ ($z$ = 0.1–1.0) semiconducting oxide glasses", *J. Appl. Phys*., **74**(2), 931-938.
Moulson, A.J. and Herbert, J.M. (2003), *Electroceramics*, 2nd Edn. John Wiley and Sons Ltd., England.
Prasad, K., Suman, C.K. and Choudhary, R.N.P. (2006), "Electrical characterization of $Pb_2Bi_3SmTi_5O_{18}$ ceramic using impedance spectroscopy", *Adv. Appl. Ceram*., **105**(5), 258-264.
Salam, R. (1990), "Trapping parameters of electronic defects states in Indium tin oxide from ac conductivity", *Phys. Status Solidi. A*, **117**(2), 535-540.
Sharma, G.D., Roy, M. and Roy, M.S. (2003), "Charge conduction mechanism and photovoltaic properties of 1,2-diazoamino diphenyl ethane (DDE) based schottky device", *Mater. Sci. Eng. B*, **104**(1-2), 15-25.
Umeri, A., Kuku, T.A., Scuor, N. and Sergo, V. (2008) "Raman investigation of the ageing of Ni-$BaTiO_3$ multilayer ceramic capacitors", *J. Mater. Sci*., **43**(3), 922-926.
Upadhyay, S., Sahu, A.K., Kumar, D. and Parkash, O. (1998), "Probing electrical conduction behavior of $BaSnO_3$", *J. Appl. Phys.*, **84**(2), 828-833.
Yuan, Y., Zhang, S. and You, W. (2004), "Preparation of $BaTiO_3$-based X7R ceramics with high dielectric constant by nanometer oxides doping method", *Mater. Lett*., **58**(12-13), 1959-1963.
Yuan, Y., Du, M., Zhang, S. and Pei, Z. (2009), "Effects of $BiNbO_4$ on the microstructure and dielectric properties of $BaTiO_3$-based ceramics", *J. Mater. Sci.-Mater. El.*, **20**(2), 157-162.

## Description of parameters

$R_p$ (profile factor) = $100[\sum|y_i\text{-}y_{ic}|/\sum|y_i|]$, where $y_i$ is the observed intensity and $y_{ic}$ is the calculated intensity at the $i^{th}$step.

$R_{wp}$ (weighted profile factor) = $100[\sum\omega_i|y_i\text{-}y_{ic}|^2/\sum\omega_i(y_i)^2]^{1/2}$, where $\omega_i = 1/\sigma_i^2$ and $\sigma_i^2$ is variance of the observation.

$R_{exp}$ (expected weighted profile factor) = $100[(n\text{-}p)/\sum\omega_i(y_i)^2]^{1/2}$,where $n$ and $p$ are the number of profile points and refined parameters, respectively.

$R_B$ (Bragg factor) = $100[\sum|I_{obs}\text{-}I_{calc}|/\sum|I_{obs}|]$, where $I_{obs}$ is the observed integrated intensity and $I_{calc}$ is the calculated integrated intensity.

$R_F$ (crystallographic $R_F$ factor) = $100[\sum|F_{obs}\text{-}F_{calc}|/\sum|F_{obs}|]$,where $F$ is the structure factor, $F = \sqrt{(I/L)}$, where $L$ is Lorentz polarization factor.

$\chi^2 = \sum\omega_i(y_i\text{-}y_{ic})^2$.

$d$ (Durbin–Watson statistics) = $\sum\{[\omega_i(y_i\text{-}y_{ic})\text{-}\omega_{i\text{-}1}(y_{i\text{-}1}\text{-}y_{ic\text{-}1})]^2\}/\sum[\omega_i(y_i\text{-}y_{ic})]^2$.

$Q_D$ = expected $d$.

$S$ (goodness of fit) = $(R_{wp}/R_{exp})$.